

Article

Biochars from Lignin-rich Residue of Furfural Manufacturing Process for Heavy Metal Ions Remediation

Baobin Wang^{1,2,3}, Miao Ran², Guigan Fang^{1,2,*}, Ting Wu² and Yonghao Ni^{3,*}

¹ College of Light Industry Science and Engineering, Nanjing Forestry University, Nanjing 210037, China; wangbaobin0408@163.com

² Key Lab. of Biomass Energy and Material, Institute of Chemical Industry of Forestry Products, CAF, Nanjing 210042, China; ranmiaolhs@163.com (M.R.); wuting@icifp.cn (T.W.)

³ Limerick Pulp and Paper Centre and Department of Chemical Engineering, University of New Brunswick, Fredericton, NB E3B 5A3, Canada

* Correspondence: fanguigan@icifp.cn (G.F.); yonghao@unb.ca (Y.N.); Tel.: +1-506-451-6857 (Y.N.); Fax: +1-506-453-4767 (Y.N.)

Received: 23 January 2020; Accepted: 21 February 2020; Published: 25 February 2020



Abstract: The pentose/furfural industrial manufacturing process uses corn cob residue as a raw material, where such a process yields significant amount of lignin-rich residue (LCR) at the end, which is commonly disposed by burning. In this study, the conversion of LCR to biochars (BCs), and their subsequent applications for heavy metal ion removal, were investigated. The BCs were prepared through hydrothermal carbonization and post-activation, using either ZnCl₂ or H₃PO₄ treatment. The as-prepared activated BCs were characterized using N₂ adsorption–desorption isotherms, XRD, FT-IR, SEM and TEM, and their performance in removing heavy metal ions (Pb²⁺, Cu²⁺, Cd²⁺) from aqueous solutions was assessed. The ZnCl₂-activated BCs (BC-ZnCl₂) exhibit a higher adsorption capacity than the H₃PO₄-activated BCs (BC-H₃PO₄), mainly due to the differences in their chemical/physical characteristics. The related adsorption kinetics and isotherms were analyzed.

Keywords: lignocellulosic residue (LCR); biochar (BC); adsorption

1. Introduction

In China, there are many commercial operations for extracting pentoses/furfural from corn cobs [1–3], and in the process, solid lignocellulosic residue (LCR), are generated at approximately 23 million tons annually [4]. Currently, the generated LCRs are burned, which is an undesirable solution; on the other hand, by following the integrated biorefinery concept [4,5], other value-added products from LCR may be produced. Accordingly, there have been many studies reported on the topic of converting LCR to useful products, including the production of porous carbon for super capacitor electrodes [6], hydrochars [7], phenols [8] and biofuels [9,10]. These studies show promising LCR-derived products that can bring alternative values to current burning practices.

Carbonaceous adsorbents (CAs) exhibit various potential applications, which include adsorption [11], catalysis [12,13], energy storage [14] and biomedicine [15]. Among them, water purification is one application that has received much attention, and is of particular interest in China [16]. CAs have favorable adsorption characteristics, e.g., high surface area, specific pore volume and surface functional groups [17]. However, the specific properties of CAs are largely dependent upon the particular activation process applied in their preparation [18,19]. Most often, ZnCl₂ and H₃PO₄ are used for the chemical activation process, which leads to the formation of chars with high porosity and surface area, thus imparting high adsorption capacity [20,21].

Many studies have been conducted regarding the removal of toxic heavy metals from water using various techniques, such as adsorption, ion exchange, membrane filtration, electrodialysis, reverse osmosis, ultrafiltration [22] and photocatalytic degradation [23]. Among them, adsorption, specifically using carbonaceous materials, is effective for water purification. In addition, by utilizing biomass residues, added value is brought to the overall process, which in turn minimizes costs, and provides an alternative method for treating solid waste [24].

In this study, a new process was developed aimed at the value-added conversion of LCRs to BCs. The process consisted of two stages: (1) a hydrothermal stage to produce hydrochar, and (2) an activation stage to obtain low-cost biochars. The hydrothermal stage was conducted under inert atmospheric conditions at 250 °C for 2 h. The activation process was performed using activating agents (H_3PO_4 , ZnCl_2) at 500 °C for 2 h. Characterization of the as-prepared biochars was performed via N_2 adsorption and desorption analysis, Fourier-transform infrared spectroscopy (FT-IR), the Boehm titration method, and X-ray diffraction (XRD). In addition, the as-prepared biochars were further tested for performance in removing Pb (II), Cd (II) and Cu (II) from aqueous solutions, and the adsorption parameters, i.e., solution pH, initial concentration, and contact time on adsorption capability, were investigated. Finally, the equilibrium isotherms and adsorption kinetics were developed.

2. Materials and Methods

Materials and Chemicals. Lead (II) nitrate ($\geq 99.99\%$), copper (II) nitrate ($\geq 99.99\%$) and cadmium (II) nitrate ($\geq 99.99\%$) were purchased from Macklin Inc. (Shanghai, China). All materials and chemicals were used as received, without any further treatment, and ultrapure water was obtained from a Hi-tech (Beijing, China) water filtration station (18.2 $\text{M}\Omega\cdot\text{cm}$ at 20 °C). The pHs of working solutions were adjusted with 0.1 M NaOH and 0.1 M HNO_3 .

Material Synthesis. LCR generated from the furfural production process was provided by Shandong Longlive Biotechnology Company (Dezhou, China), and was then used to prepare biochars (the BC- H_3PO_4 : H_3PO_4 biochar and the BC- ZnCl_2 : ZnCl_2 biochar). The chemical composition (mass basis) of the CCR consisted of: cellulose (72.3%), lignin (16.2%), hemicellulose (7.2%), extractives (8.1%) and ash (4.2%), and was determined in accordance with TAPPI standard methods (T 201, T 222, T 223, T 204 and T 211, respectively).

As depicted in Figure 1, the preparation of the biochar material was performed using three steps, these being pretreatment, carbonization and activation.

Pretreatment. Initially, the LCR was dried to a constant weight under room temperature, and subsequently milled to a particle size of below 100 mesh (0.15 mm), sieved, and then stored in a sealed bag.

Carbonization. The hydrothermal carbonization process was performed according to the following procedures [7]: 5 g (odw) of LCR and 50 mL of distilled water were loaded into a 250 mL Parr stirred pressured reactor (4576A, Parr instrument company, Moline, IL, USA). Next, the reactor was sealed, flushed with N_2 , and heated to 250 °C for 2 h to carbonize the sample. These carbonized samples were then removed from the reactor and washed with ethanol and water until the wash filtrate was neutral. The final product obtained from the carbonization process was denoted as “hydrochar”.

Activation. The hydrochar was mixed with an aqueous solution of 40% H_3PO_4 with the ratio of hydrochar/ H_3PO_4 at 1:6 (kg/kg), allowing the treatment for 24 h at room temperature. Subsequently, the mixture was transferred to a tube furnace, which was flushed using N_2 . The mixture was then heated at a rate of 10 °C/min, until the desired activation temperature reached 500 °C, and this was maintained for 2 h, followed by cooling inside the furnace to room temperature. After cooling, the activated mixture was washed several times with hot, distilled water (60 °C) until a neutral pH was achieved. After washing, the sample was then dried at 105 °C in an oven for 8 h, and was labeled as BC- H_3PO_4 .

To prepare the product BC- ZnCl_2 , hydrochar was activated instead using ZnCl_2 in a similar fashion as to the BC- H_3PO_4 product. To do this, the hydrochar was mixed with an aqueous solution

of 40% ZnCl_2 with a ratio of 1:10 (kg/kg), and placed into a cupel for a duration of 24 h at room temperature. The subsequent heating of the sample was performed identically to the heating process performed for $\text{BC-H}_3\text{PO}_4$. The activated product was then boiled with a volume of 1 M HCl equaling 10 times the volume of the hydrochar for a duration of 1 h. Next, the activated mixture was washed several times with hot, distilled water (60 °C) until the filtrate was absent of chloride ions. The sample was then dried at 105 °C in an oven for 8 h after washing, and was labeled BC-ZnCl_2 .

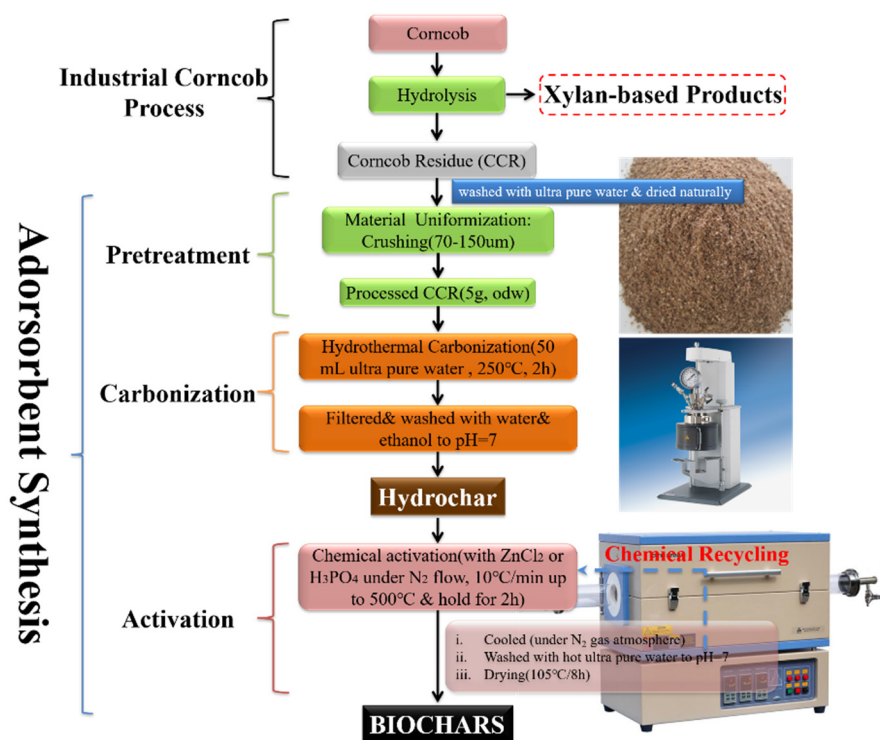


Figure 1. Synthesis procedures for preparing biochar (BC) samples: BC-ZnCl_2 and $\text{BC-H}_3\text{PO}_4$.

2.1. Adsorption Experiment

The effect of the solution's pH was investigated by adjusting the starting pH of the metal ion solution prior to commencing the experiment. Initially, a metal ion concentration of 1.0 mM was prepared and allowed to reach equilibrium over a duration of 10 h. The initial pH of the solution was then adjusted within a pH range of 2.0 to 6.0 by adding appropriate amounts of 0.1 M NaOH or 0.1 M HNO_3 . The maximum tested pH value was fixed at 6.0 to avoid the precipitation of metal ions that can occur at higher pH values.

Equilibrium experiments were conducted at isothermal conditions of 25 ± 2 °C as a batch process. To develop adsorption equilibrium isotherms, 0.6 g of BC samples were placed into 250 mL Erlenmeyer flasks containing 100 mL of metal ion solutions, having different initial concentrations within the range of 0.5 to 5.0 mM for Pb (II), Cd (II) and Cu (II) metal ions at optimal pH conditions. The flasks containing the BC samples and metal ions were then continuously agitated at 6.67 Hz for 10 h. The samples were then filtered through a 0.45 mm cellulose filter paper, and metal concentrations of the filtrate were analyzed. Metal ion concentrations within solutions were analyzed using the atomic absorption spectrum (Shimadzu AA6701F, Kyoto, Japan).

2.2. Characterization of Carbon Materials

The crystallinity of samples was determined using X-ray diffraction (XRD) (D8-ADVANCE, Bruker, Bremen, Germany) with $\text{Cu K}\alpha$ radiation at 10 kV. The XRD data was collected from 10 to 80° (θ) at a scan rate of 2°/min. The surface area was calculated using the Brunauer–Emmett–Teller (BET) method.

The pore volume was determined from the amount of N_2 adsorbed at $P/P_0 = 0.98$. The surface functional groups and adsorptive form of heavy metals were identified using IR spectroscopy. The reflectance infrared spectra were obtained using a Shimadzu FT-IR spectrophotometer (Kyoto, Japan), where each spectrum was recorded over a wavenumber range of $500\text{--}4000\text{ cm}^{-1}$. Oven-dried KBr pellets were used for sample preparation.

3. Results

3.1. Concept of Preparing Biochars from LCR for the Removal of Heavy Metal Ions

As illustrated in Figure 2, LCR was hydrothermally carbonized ($250\text{ }^\circ\text{C}$, 2 h) first to hydrochar. Subsequently, the hydrochar was chemically activated using either H_3PO_4 or $ZnCl_2$ as the activating agent. Finally, the biochar products were used for metal ion removal from aqueous solutions through an adsorption mechanism.



Figure 2. Concept of Biochars preparation and their applications for heavy metal ion removal through adsorption mechanisms.

A high surface area and porous structure of the biochar are key parameters for efficient metal ion removal based on the adsorption concept. A porous structure allows metal ions to easily diffuse within the biochar, which facilitates the adsorption process. Moreover, as metal ions diffuse into the porous network, a high surface area improves the availability of functional groups for metal ions interaction. There are two main mechanisms of adsorption that occur in this process: (a) the acid groups (carboxyl ($-\text{COOH}$), phenolic groups (R-OH)) of the biochar will interact with the metal ions; and (b) the aromatic structures formed in the biochar due to graphitization can act as π donors, and as a result, cationic metal ions will interact with the aromatic rings (i.e., through the cation- π interactions). Both mechanisms play an important role in the metal ion removal during the sorption process.

3.2. Physicochemical Characterizations

The nitrogen sorption isotherms of hydrochar and the prepared bio-based activated carbons are presented in Figure 3a. The N_2 adsorption/desorption isotherms of the BC- H_3PO_4 and BC- $ZnCl_2$ samples resemble the typical Type I isotherm, and a plateau occurs at low relative pressure with a predominance of micropores in the sorbent, followed by continuing N_2 adsorption into the mesopores once the micropores are saturated [25,26]. The N_2 isotherms also demonstrate a small hysteresis loop

in the desorption curve, which implies the presence of mesopores, with the possible occurrence of a capillary condensation phenomenon.

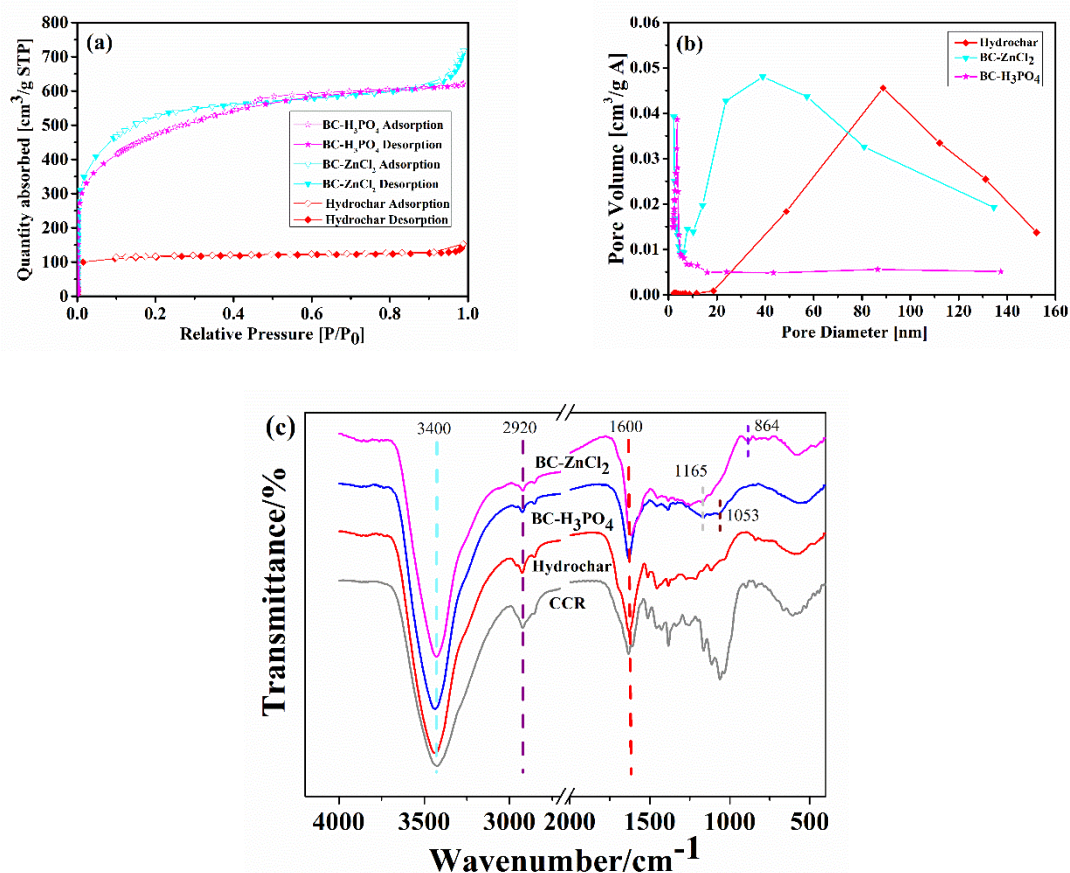


Figure 3. Physicochemical properties of the Biochars. (a) Nitrogen adsorption and desorption isotherms of Hydrochar, BC-H₃PO₄ and BC-ZnCl₂ at 98 K; (b) Pore size distribution of Hydrochar, BC-H₃PO₄ and BC-ZnCl₂; (c) FT-IR spectra of CCR, Hydrochar, BC-H₃PO₄ and BC-ZnCl₂.

The pore distribution of the hydrochar, BC-H₃PO₄ and BC-ZnCl₂ samples are shown in Figure 3b. The pore size distribution curve of BC-H₃PO₄ shows a microporous structure, while the combined micropores/mesopores are for the BC-ZnCl₂ sample.

The BET surface area and pore volume of the hydrochar, BC-H₃PO₄ and BC-ZnCl₂ samples are shown in Table 1. The results show that the H₃PO₄ and ZnCl₂ treatments during the activation process are effective for producing activated carbons with increased high surface area (790 m²/g for BC-ZnCl₂ and 680 m²/g for BC-H₃PO₄) and high pore volume (0.74 cm³/g for BC-ZnCl₂ and 0.65 cm³/g for BC-H₃PO₄). Interestingly, the BC-ZnCl₂ sample demonstrated higher BET surface area and pore volume compared to the BC-H₃PO₄ sample. The results from the BET analysis correlate well with those found in the literature regarding H₃PO₄ and ZnCl₂ activating treatment. For example, Myglovets et al. reported that the surface area of lignosulfonate-based carbons does attain 1370 m²/g after phosphoric acid activation at 1000 °C [27]. In addition, a tomato processing waste-based char was obtained with high BET surface area (1093 m²/g) after zinc chloride activation [28].

The functional groups on the surface of the biochars were determined using the Boehm titration method; the results are presented in Table 1. Clearly, the BC-ZnCl₂ sample had more functional groups than the BC-H₃PO₄ sample. The acidic groups (carbonyl, carboxylic, lactones and phenol groups) content in the BC-ZnCl₂ and BC-H₃PO₄ samples were 0.98 and 0.69 mmol/g, respectively. It was reported that 50% H₃PO₄ and 75% ZnCl₂ impregnation generates approximately 5.6 mmol/g and 2 mmol/g acidic groups, respectively, in the activated carbon [29].

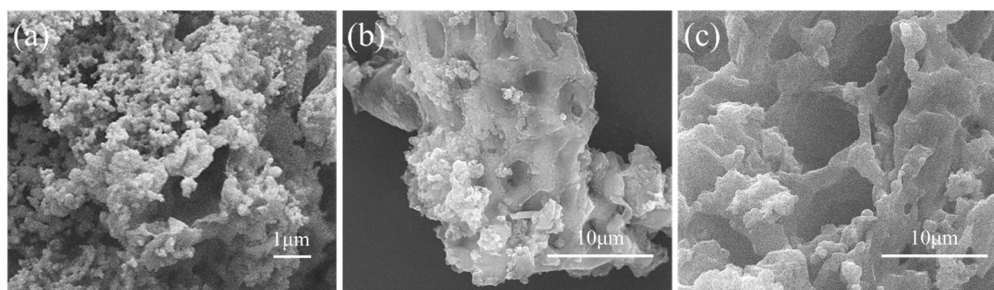
Table 1. Summary of properties for Hydrochar, BC-H₃PO₄ and BC-ZnCl₂.

Properties	Hydrochar	BC-H ₃ PO ₄	BC-ZnCl ₂
pH _{pzc}	9.8	3.5	4.6
BET surface Area (m ² /g)	13.2	680	790
Pore volume (cm ³ /g)	0.068	0.65	0.74
Boehm Titration	Carbonyl/ (mmol/g)	-	0.095
	Carboxylic/ (mmol/g)	-	0.082
	Lactones/ (mmol/g)	-	0.065
	Phenolics/ (mmol/g)	-	0.45
	Basicity/ (mmol/g)	-	0.21

FT-IR characteristics of the raw material (LCR), hydrochar and the BC-ZnCl₂ and BC-H₃PO₄ samples, are shown in Figure 3c. The CCR samples showed similar features to regular lignocellulosic materials: hydroxyl groups (~3400 cm⁻¹), C–H stretching from –CH₂ groups (2920 cm⁻¹), C–O stretching (1000–1350 cm⁻¹), C–O–C stretching (~1164 cm⁻¹) and glycosidic linkages (~895 cm⁻¹) [30]. After the hydrocarbonization process, many of these functional groups disappeared. The biochar samples showed a wide band at approximately 3400 cm⁻¹, which can be associated with the OH stretching vibration mode in alcohol and phenol.

For the BC-ZnCl₂ sample, the band located at about 1600 cm⁻¹ is attributable to C=C vibrations, those at 1720 cm⁻¹, 1165 cm⁻¹ and 864 cm⁻¹ are due to C=O, C–O, and C–H vibrations, respectively [31]. For the BC-H₃PO₄-hydrochar sample, the bands at 1160–1180 cm⁻¹, 1060 cm⁻¹ and 950–990 cm⁻¹ are attributed to the presence of phosphorus species [27]. The band at 1720 cm⁻¹ is assigned to the stretching mode of carboxylic bonds [32]. Those at around 1150–1180 cm⁻¹ can be assigned to C–O stretching vibrations in a C–O–P (aromatic) linkage, to stretching vibrations of hydrogen-bonded P=O groups of phosphates or polyphosphates, and to P=OOH. The band at 1053 cm⁻¹ may represent the P–O–P vibrations. FT-IR results demonstrated that these activated biocarbon samples are rich in the functional groups.

The surface morphology of hydrochar, BC-H₃PO₄ and BC-ZnCl₂ samples are shown in the SEM images (Figure 4). The melted surface and irregular pores were evident for the hydrochar sample, while BC-ZnCl₂ and BC-H₃PO₄ samples exhibited heterogeneous, well developed porous structures. Comparatively, Angin found well-developed, porous structures for the ZnCl₂-activated biochars that were produced from sour cherry stones [33]. Lastly, in accordance with the XRD pattern (Figure S1), the peaks at 26° and 43° are assigned to disordered graphitic (002) and (10) plane, respectively. The as-prepared biochar samples demonstrated typical broad peaks, indicating that the samples have a low crystalline degree.

**Figure 4.** Scanning electron microscopy (SEM) images of (a) 500× Hydrochar; (b) 5000× BC-H₃PO₄; (c) 5000× BC-ZnCl₂.

The point of zero charge (pH_{pzc}) (Table 1) was determined by analyzing the zeta potential charge when varying the pH range from 2 to 8. As shown, for the LCR sample, the pH_{pzc} is 9.8, while the pH_{pzc} of BC-H₃PO₄ and BC-ZnCl₂ are 3.5 and 4.6, respectively. These results confirm the presence of these

acid groups on the surface of activated carbons. Figure 5 exhibits the adsorption of Pb^{2+} under various pH. The adsorption amount of Pb^{2+} increased when the pH increased. The maximum adsorption amount (75.3 mg/g) was achieved at the pH of 5–6. When the pH is over 6, the metal precipitation would dominate, thus the adsorption of metal ions should be controlled [34]. The adsorption amount was minimal at low pHs (1–3), while the adsorption increased at elevated pHs (4–5). The metal ions will replace protons from the biochar at elevated pHs. When the pH is higher than the pH_{pzc} , the surface of the sorbent is negatively charged, and attractive forces increase between the sorbent surface and metal ions. Furthermore, a higher pH favors the deprotonation of the sorbents' phenolic and carboxylic acid groups, and thus, negative sites are created on both BC- $ZnCl_2$ and BC- H_3PO_4 surfaces, thereby improving the adsorption of metal ions onto the surface of the sorbents. Mohan et al. [34] reported that the final pH of the solution is higher than the initial pH under acidic conditions, as neutralization and sorption are parallel processes; therefore, a pH of 5 was chosen as the optimal pH for performing the adsorption process.

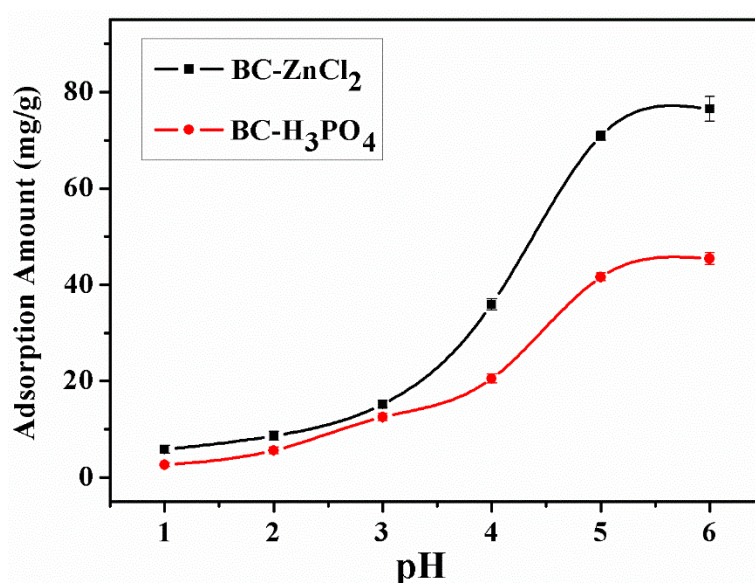


Figure 5. Adsorption amount of Pb^{2+} with various pHs.

4. Discussion

4.1. Adsorption Kinetics

Figure 6a,b presented the adsorption analyses of Pb (II) onto the two BC samples. The process was very fast, and during the first 30 min, the uptake of Pb (II) was over 90% of the equilibrium amount, and the equilibrium was attained at approximately 4 h. Fast adsorption was also observed for the adsorption of Cd (II) and Cu (II) in the first 30 min (Figure S2). In the literature [35] it was reported that activated carbon prepared from marine green algae demonstrates high adsorption rates, and more than 90% of the equilibrium amount of Pb (II) ions are removed within the first 30 min. Furthermore, there are two adsorption kinetic regions during the adsorption process. Initially, there is a high adsorption rate region, which is associated with the large number of available active adsorption sites, and the high driving force facilitates the rapid adsorption of metal ions onto the active sites. The slow second region is due to the metal ion diffusion into the porous structure.

The adsorption kinetics of heavy metal ions is related to the physical and/or chemical properties of activated carbons. Three models, namely, the pseudo-first-order (PFO), pseudo-second-order (PSO) and intra-particle diffusion model (IPD), were applied to the kinetic data. The fitting parameters associated with the three models for Pb (II) are presented in Table 2.

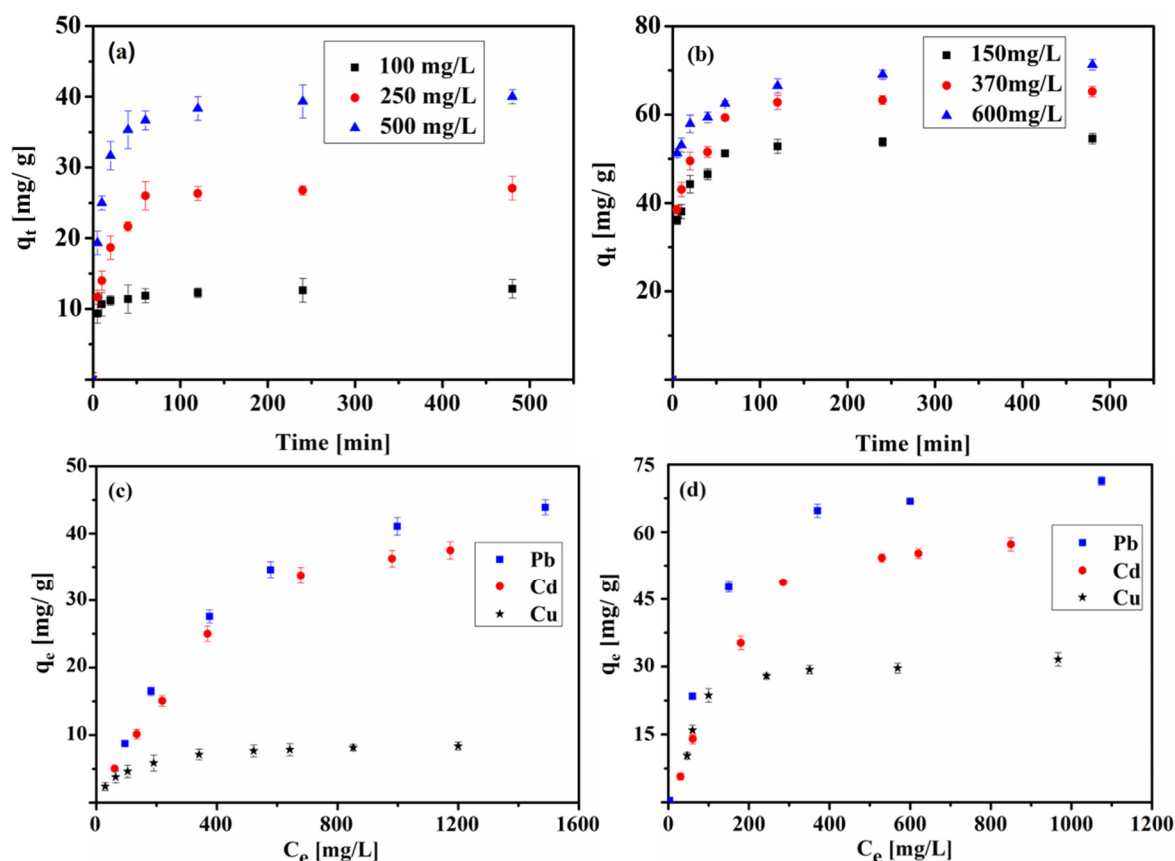


Figure 6. Kinetic analyses of Pb (II) adsorption on (a) BC-H₃PO₄ as a function of contact time; (b) BC-ZnCl₂ as a function of contact time; Adsorption isotherms of Pd (II), Cd (II) and Cu (II) on (c) BC-H₃PO₄ and (d) BC-ZnCl₂.

Table 2. Kinetic fitting parameters of pseudo-first-order (PFO), pseudo-second-order (PSO) and intra-particle diffusion (IP) models for BC-H₃PO₄ and BC-ZnCl₂ removal of Pb (II).

C ₀	q _{exp}	PFO			PSO			IPD		
		Q ₁	K ₁	R ²	Q ₂	K ₂	R ²	K _i	C	R ²
BC-H₃PO₄										
100 mg/L	11.5	9.7	0.045	0.854	11.8	0.0079	1.000	1.06	22.22	0.299
250 mg/L	25.8	28.2	0.064	0.914	24.9	0.0019	0.999	3.08	32.61	0.563
500 mg/L	39.7	38.0	0.061	0.898	39.9	0.0017	1.000	4.13	55.37	0.481
BC-ZnCl₂										
150 mg/L	51.2	55.4	0.011	0.852	51.1	0.0092	1.000	3.45	41.74	0.408
370 mg/L	60.9	68.5	0.0093	0.842	60.7	0.0051	1.000	3.08	54.50	0.484
600 mg/L	65.3	69.6	0.0081	0.854	65.2	0.0057	0.999	4.13	89.56	0.377

Fitting parameters for Cd (II) and Cu (II) were also analyzed, as shown in Tables S1 and S2. The results show that the experimental data agrees with the PSO model (R² near unity). In addition, the predicted values (Q) obtained from the PSO model are in accordance with the experimental q_{exp} values.

4.2. Adsorption Isotherms

The adsorption isotherms of heavy metal ions are shown in Figure 4c,d (at 25 °C). For the BC-ZnCl₂ sample, the adsorption uptake of Pb (II), Cd (II) and Cu (II) are 23.1–72.1 mg/g, 6.8–55.6 mg/g

and 8.2–30.5 mg/g, respectively, which is highly dependent upon the initial concentration of these metal ions.

In comparison, Barczak et al. reported that heavy metal ion (Pb, Zn, Cu, Cd) adsorption isotherms for well-ordered carbons obtained from the hard templating of SBA-15 shows dependency on the initial concentration of the solution [36]. Additionally, the adsorption isotherms show an L-type according to Giles's classification [37], indicating high adsorbate–adsorbent interactions.

The Freundlich (Equation (1)) and Langmuir (Equation (2)) isotherm models were used to fit the adsorption equilibrium experimental data.

$$\ln q_e = \ln K_F + \ln C_e/n \quad (1)$$

$$C_e/q_e = 1/q_m K + C_e/q_m \quad (2)$$

where C_e is the metal ions concentration (mg/L) at equilibrium, q_e is the adsorption capacity at equilibrium (mg/L), K_F (L/mg) is the Freundlich constant, $1/n$ is the heterogeneity factor, and K (L/mg) and q_m (mg/g) are the Langmuir coefficients, representing the adsorption equilibrium constant and the monolayer capacity, respectively.

The Langmuir isotherm assumes monolayer sorption on a surface with a finite number of identical sites and uniform adsorption energies [38], while the Freundlich isotherm assumes that the adsorption occurs on a heterogeneous surface by multilayer adsorption, and the amount of adsorbate adsorbed increases infinitely with the increase of its concentration [39]. Table 3 depicts the fitting data of the equilibrium experimental data. The Langmuir isotherm gave a stronger fitting correlation constant (R^2) in the range of 0.98–1.00, which is compared to that of the Freundlich isotherm in the range of 0.73–0.96. The BC-ZnCl₂ sample exhibited a better adsorption capacity than the BC-H₃PO₄ sample for the three metal ions studied. These results are in agreement with those from the Boehm titration method, in that more acid groups facilitate electrostatic interactions, thereby increasing the adsorption capacity.

Table 3. Isotherms fitting parameters of the Freundlich and Langmuir models for the BC-H₃PO₄ and BC-ZnCl₂ removals of Pd (II), Cd (II) and Cu (II).

Biochar Type	Freundlich Model			Langmuir Model				
	K_F (L/mg)	n	R^2	q_m (mg/g)	K (L/mg)	R^2	R_L	
BC-H ₃ PO ₄	Cu (II)	3.71	3.02	0.93	7.2	0.54	1.00	0.002
	Cd (II)	1.38	1.45	0.96	36.9	0.072	1.00	0.011
	Pb (II)	2.92	1.71	0.93	44.8	0.014	0.99	0.324
BC-ZnCl ₂	Cu (II)	6.37	3.15	0.73	27.5	0.15	0.99	0.105
	Cd (II)	4.09	1.47	0.90	50.4	0.036	0.98	0.495
	Pb (II)	8.13	2.62	0.82	63.5	0.089	0.98	0.134

The relative adsorption tendency can be quantified by the separation factor, R_L as defined in Equation (3) [40].

$$R_L = 1/(1 + K_L C_0) \quad (3)$$

where K_L is the Langmuir constant (L/mg) expressed in Equation (1), and C_0 is the initial metal ion concentration (mg/L). It is well known that values in the range of $0 < R_L < 1$ represent favorable adsorption [41]. The fitted results at equilibrium yield the R_L values in a range of 0.002 to 0.495, indicating favorable adsorption performances for the as-prepared adsorbents.

The concept of the biomass-derived biochar preparation for heavy metal ions removal is shown in Figure 7. In our previous study, corn cob residue was first utilized for the preparation of hydrochar through hydrothermal carbonization, which can be utilized for fuel, and then bio-oil can be obtained in this process. In order to convert the solid residue problem in this process, biochar was fabricated through a further chemical activation process. The carbon yield for BC-ZnCl₂ and BC-H₃PO₄ is 35.9%

and 32.4%, respectively. In addition, the chemicals could be recycled for activation in the next cycle (Figure 1). The as-prepared biochars were used for heavy metal ions removal. The adsorption amount for BC-ZnCl₂ and BC-H₃PO₄ is 72.1 mg/g and 42.7 mg/g, respectively.

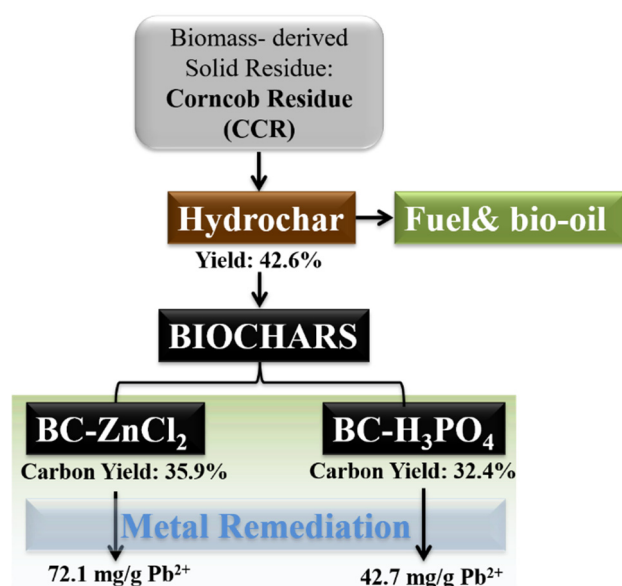


Figure 7. Concept of the biomass-derived biochar for Pb²⁺ remediation.

Thus, BC-ZnCl₂ is recognized as a better process for the concept. We believe the biochar preparation process expanded the conversion and utilization of biomass-derived solid residue.

4.3. Summary of Pb (II) Adsorption Capacities for Different Carbonaceous Materials

Table 4 summarizes the adsorption capacities for Pb (II) of different carbonaceous materials. Compared to other recently reported carbonaceous materials, the as-prepared BC-ZnCl₂ and BC-H₃PO₄ samples exhibit excellent Pb (II) removal capacity via adsorption. As well as this, BC-ZnCl₂ exhibited a low cost, effective biochar compared with other functionalized/modified biochars.

Table 4. Summary of the Pb (II) adsorption capacities of different carbonaceous materials.

Absorbent Used	Q Ads (mg/g)	References
Banana peel-activated carbon	34.5	[42]
Sugarcane cane biochar	86.9	[43]
Raw sugarcane bagasse biochar	81.9	[44]
Functionalized Porous lignin	188	[45]
Graphene/activated carbon composite	212	[28]
KMnO ₄ -treated hickory wood biochar	153.1	[46]
This study (BC-H ₃ PO ₄)	42.7	this study
This study (BC-ZnCl ₂)	72.1	this study

5. Conclusions

In this study, two biochar samples, BC-H₃PO₄ and BC-ZnCl₂, were prepared from corn cob residue through a hydrothermal carbonization and subsequent chemical activation process. The biochars exhibit well-developed porous structures, with high BET surface areas (up to 790 m²/g for BC-ZnCl₂) and acid groups. These are desirable features in regard to the removal of heavy metal ions from aqueous solutions.

The biochars show excellent adsorption capacities for heavy metal ions removal. The main mechanisms for metal ions removal include porous diffusion, electrostatic interactions and cation- π

interactions. The BC-ZnCl₂ sample demonstrates higher adsorption capacities than the BC-H₃PO₄ sample, due to its higher amount of acid groups (0.98 mmol/g vs 0.69 mmol/g), higher surface area (790 m²/g vs 680 m²/g), and higher porosity (0.74 cm³/g vs 0.65 cm³/g).

The adsorption process is of a chemisorption nature, as indicated by the strong correlation between a pseudo-second-order model and the experimental data. Adsorption uptakes of Pb (II), Cd (II) and Cu (II) for the BC-ZnCl₂ sample, which increase with the initial concentrations (0.5–5.0 mmol/L), are 23.1–72.1 mg/g, 6.8–55.6 mg/g and 8.2–30.5 mg/g, respectively. The isotherm adsorption data agree with the Langmuir model, these results support the conclusion that the developed biochars present a promising potential for heavy metal removal for water purification and treatment applications.

Supplementary Materials: The following are available online at <http://www.mdpi.com/1996-1944/13/5/1037/s1>, Figure S1. SEM images of (a) 500×Hydrochar; (b) 5000×BC-H₃PO₄; (c) 4800×BC-ZnCl₂. Figure S2. XRD of Hydrochar, BC-H₃PO₄ and BC-ZnCl₂. Table S1. Kinetic fitting parameters of the PFO, PSO and IPD models for the BC-H₃PO₄ removal of Cd (II) and Cu (II). Table S2. Kinetic fitting parameters of the PFO, PSO and IPD models for the BC-ZnCl₂ removal of Cd (II) and Cu (II).

Author Contributions: Conceptualization, B.W., G.F. and Y.N.; methodology, B.W.; software, M.R.; validation, M.R., T.W. and G.F.; formal analysis, B.W.; investigation, B.W.; resources, B.W.; data curation, B.W.; writing—original draft preparation, B.W.; writing—review and editing, B.W. and G.F.; visualization, M.R.; supervision, G.F. and Y.N.; project administration, G.F.; funding acquisition, G.F. All authors have read and agreed to the published version of the manuscript.

Funding: The work was supported by the National Key Research and Development Program of China (2017YFD0601005). The author is grateful for the support of China Scholarship Council (CSC) and New Brunswick Innovation Funding (NBIF).

Conflicts of Interest: The authors declare no conflict of interest.

References

- Hromadkova, Z.; Kováčiková, J.; Ebringerová, A. Study of the classical and ultrasound-assisted extraction of the corn cob xylan. *Ind. Crops Prod.* **1999**, *9*, 101–109. [[CrossRef](#)]
- Tan, S.; Li, D.; Jiang, Z.; Zhu, Y.; Shi, B.; Li, L. Production of xylobiose from the autohydrolysis explosion liquor of corncob using *Thermotoga maritima* xylanase B (XynB) immobilized on nickel-chelated Eupergit C. *Bioresour. Technol.* **2008**, *99*, 200–204. [[CrossRef](#)]
- Yao, D.; Ma, P.; Wang, Y.; Yang, J.; Zhang, L.-Y. Optimization of extraction process for xylan from corncob by response surface methodology. *Food Sci.* **2011**, *8*, 25.
- Bu, L.; Xing, Y.; Yu, H.; Gao, Y.; Jiang, J. Comparative study of sulfite pretreatments for robust enzymatic saccharification of corn cob residue. *Biotechnol. Biofuels* **2012**, *5*, 87. [[CrossRef](#)] [[PubMed](#)]
- Kong, F.; Wang, S.; Price, J.T.; Konduri, M.K.; Fatehi, P. Water soluble kraft lignin–acrylic acid copolymer: Synthesis and characterization. *Green Chem.* **2015**, *17*, 4355–4366. [[CrossRef](#)]
- Qu, W.-H.; Xu, Y.-Y.; Lu, A.-H.; Zhang, X.-Q.; Li, W.-C. Converting biowaste corncob residue into high value added porous carbon for supercapacitor electrodes. *Bioresour. Technol.* **2015**, *189*, 285–291. [[CrossRef](#)] [[PubMed](#)]
- Zhang, L.; Wang, Q.; Wang, B.; Yang, G.; Lucia, L.A.; Chen, J. Hydrothermal carbonization of corncob residues for hydrochar production. *Energy Fuels* **2015**, *29*, 872–876. [[CrossRef](#)]
- Jiang, Z.; He, T.; Li, J.; Hu, C. Selective conversion of lignin in corncob residue to monophenols with high yield and selectivity. *Green Chem.* **2014**, *16*, 4257–4265. [[CrossRef](#)]
- Liu, K.; Lin, X.; Yue, J.; Li, X.; Fang, X.; Zhu, M.; Lin, J.; Qu, Y.; Xiao, L. High concentration ethanol production from corncob residues by fed-batch strategy. *Bioresour. Technol.* **2010**, *101*, 4952–4958. [[CrossRef](#)]
- Yu, G.; Xu, H.; Liu, C.; DeRoussel, P.; Zhang, C.; Zhang, Y.; Li, B.; Wang, H.; Mu, X. Ameliorated enzymatic saccharification of corn stover with a novel modified alkali pretreatment. *J. Bioresour. Bioprod.* **2016**, *1*, 42–47.
- Godwin, P.; Pan, Y.; Xiao, H.; Afzal, M.T. Progress in the preparation and application of modified biochar for improving heavy metal ion removal from wastewater. *J. Bioresour. Bioprod.* **2019**, *4*, 31–42.
- Guo, D.; Shibuya, R.; Akiba, C.; Saji, S.; Kondo, T.; Nakamura, J. Active sites of nitrogen-doped carbon materials for oxygen reduction reaction clarified using model catalysts. *Science* **2016**, *351*, 361–365. [[CrossRef](#)] [[PubMed](#)]

13. Li, J.; Wang, X.; Chen, G.; Li, D.; Zhou, Y.; Yang, X.; Wang, J. Hypercrosslinked organic polymer based carbonaceous catalytic materials: Sulfonic acid functionality and nano-confinement effect. *Appl. Catal. B Environ.* **2015**, *176*, 718–730. [[CrossRef](#)]
14. Zhao, X.; Li, W.; Kong, F.; Chen, H.; Wang, Z.; Liu, S.; Jin, C. Carbon spheres derived from biomass residue via ultrasonic spray pyrolysis for supercapacitors. *Mater. Chem. Phys.* **2018**, *219*, 461–467. [[CrossRef](#)]
15. Chen, Y.; Xu, P.; Wu, M.; Meng, Q.; Chen, H.; Shu, Z.; Wang, J.; Zhang, L.; Li, Y.; Shi, J. Colloidal RBC-shaped, hydrophilic, and hollow mesoporous carbon nanocapsules for highly efficient biomedical engineering. *Adv. Mater.* **2014**, *26*, 4294–4301. [[CrossRef](#)]
16. Tao, T.; Xin, K. A sustainable plan for China's drinking water: Tackling pollution and using different grades of water for different tasks is more efficient than making all water potable. *Nature* **2014**, *511*, 527–529. [[CrossRef](#)]
17. De Gisi, S.; Lofrano, G.; Grassi, M.; Notarnicola, M. Characteristics and adsorption capacities of low-cost sorbents for wastewater treatment: A review. *Sustain. Mater. Technol.* **2016**, *9*, 10–40. [[CrossRef](#)]
18. Arenas, E.; Chejne, F. The effect of the activating agent and temperature on the porosity development of physically activated coal chars. *Carbon* **2004**, *42*, 2451–2455. [[CrossRef](#)]
19. Cazetta, A.L.; Vargas, A.M.; Nogami, E.M.; Kunita, M.H.; Guilherme, M.R.; Martins, A.C.; Silva, T.L.; Moraes, J.C.; Almeida, V.C. NaOH-activated carbon of high surface area produced from coconut shell: Kinetics and equilibrium studies from the methylene blue adsorption. *Chem. Eng. J.* **2011**, *174*, 117–125. [[CrossRef](#)]
20. Diaz-Diez, M.; Gómez-Serrano, V.; González, C.F.; Cuerda-Correa, E.; Macías-García, A. Porous texture of activated carbons prepared by phosphoric acid activation of woods. *Appl. Surf. Sci.* **2004**, *238*, 309–313. [[CrossRef](#)]
21. Şahin, Ö.; Saka, C.; Ceyhan, A.A.; Baytar, O. Preparation of high surface area activated carbon from *Elaeagnus angustifolia* seeds by chemical activation with ZnCl₂ in one-step treatment and its iodine adsorption. *Sep. Sci. Technol.* **2015**, *50*, 886–891. [[CrossRef](#)]
22. Ahsan, L.; Jahan, M.S.; Ni, Y. Recovering/concentrating of hemicellulosic sugars and acetic acid by nanofiltration and reverse osmosis from prehydrolysis liquor of kraft based hardwood dissolving pulp process. *Bioresour. Technol.* **2014**, *155*, 111–115. [[CrossRef](#)] [[PubMed](#)]
23. Gunatilake, S. Methods of removing heavy metals from industrial wastewater. *Methods* **2015**, *1*, 14.
24. Maneerung, T.; Liew, J.; Dai, Y.; Kawi, S.; Chong, C.; Wang, C.-H. Activated carbon derived from carbon residue from biomass gasification and its application for dye adsorption: Kinetics, isotherms and thermodynamic studies. *Bioresour. Technol.* **2016**, *200*, 350–359. [[CrossRef](#)] [[PubMed](#)]
25. Kołodyńska, D.; Krukowska, J.; Thomas, P. Comparison of sorption and desorption studies of heavy metal ions from biochar and commercial active carbon. *Chem. Eng. J.* **2017**, *307*, 353–363. [[CrossRef](#)]
26. Rouquerol, J.; Rouquerol, F.; Llewellyn, P.; Maurin, G.; Sing, K.S. *Adsorption by Powders and Porous Solids: Principles, Methodology and Applications*; Academic Press: Cambridge, MA, USA, 2013.
27. Myglovets, M.; Poddubnaya, O.I.; Sevastyanova, O.; Lindström, M.E.; Gawdzik, B.; Sobiesiak, M.; Tsyba, M.M.; Sapsay, V.I.; Klymchuk, D.O.; Puziy, A.M. Preparation of carbon adsorbents from lignosulfonate by phosphoric acid activation for the adsorption of metal ions. *Carbon* **2014**, *80*, 771–783. [[CrossRef](#)]
28. Saeidi, N.; Parvini, M.; Niavarani, Z. High surface area and mesoporous graphene/activated carbon composite for adsorption of Pb (II) from wastewater. *J. Environ. Chem. Eng.* **2015**, *3*, 2697–2706. [[CrossRef](#)]
29. Boudrahem, F.; Soualah, A.; Aissani-Benissad, F. Pb (II) and Cd (II) removal from aqueous solutions using activated carbon developed from coffee residue activated with phosphoric acid and zinc chloride. *J. Chem. Eng. Data* **2011**, *56*, 1946–1955. [[CrossRef](#)]
30. Gupta, V.; Carrott, P.; Singh, R.; Chaudhary, M.; Kushwaha, S. Cellulose: A review as natural, modified and activated carbon adsorbent. *Bioresour. Technol.* **2016**, *216*, 1066–1076.
31. Liou, T.-H. Development of mesoporous structure and high adsorption capacity of biomass-based activated carbon by phosphoric acid and zinc chloride activation. *J. Chem. Eng.* **2010**, *158*, 129–142. [[CrossRef](#)]
32. Dichiaro, A.B.; Webber, M.R.; Gorman, W.R.; Rogers, R.E. Removal of copper ions from aqueous solutions via adsorption on carbon nanocomposites. *ACS Appl. Mater. Interfaces* **2015**, *7*, 15674–15680. [[CrossRef](#)] [[PubMed](#)]
33. Angin, D. Production and characterization of activated carbon from sour cherry stones by zinc chloride. *Fuel* **2014**, *115*, 804–811. [[CrossRef](#)]

34. Mohan, D.; Kumar, H.; Sarswat, A.; Alexandre-Franco, M.; Pittman Jr, C.U. Cadmium and lead remediation using magnetic oak wood and oak bark fast pyrolysis bio-chars. *Chem. Eng. J.* **2014**, *236*, 513–528. [[CrossRef](#)]
35. Jeyakumar, R.S.; Chandrasekaran, V. Adsorption of lead (II) ions by activated carbons prepared from marine green algae: Equilibrium and kinetics studies. *Int. J. Ind. Chem.* **2014**, *5*, 2. [[CrossRef](#)]
36. Barczak, M.; Michalak-Zwierz, K.; Gdula, K.; Tyszczyk-Rotko, K.; Dobrowolski, R.; Dąbrowski, A. Ordered mesoporous carbons as effective sorbents for removal of heavy metal ions. *Microporous Mesoporous Mater.* **2015**, *211*, 162–173. [[CrossRef](#)]
37. Giles, C.H.; Smith, D.; Huitson, A. A general treatment and classification of the solute adsorption isotherm. I. Theoretical. *J. Colloid Interface Sci.* **1974**, *47*, 755–765. [[CrossRef](#)]
38. Repo, E.; Warchol, J.K.; Kurniawan, T.A.; Sillanpää, M.E. Adsorption of Co (II) and Ni (II) by EDTA-and/or DTPA-modified chitosan: Kinetic and equilibrium modeling. *Chem. Eng. J.* **2010**, *161*, 73–82. [[CrossRef](#)]
39. Jain, M.; Garg, V.; Kadirvelu, K. Chromium (VI) removal from aqueous system using Helianthus annuus (sunflower) stem waste. *J. Hazard. Mater.* **2009**, *162*, 365–372. [[CrossRef](#)] [[PubMed](#)]
40. Wu, C.-H. Adsorption of reactive dye onto carbon nanotubes: Equilibrium, kinetics and thermodynamics. *J. Hazard. Mater.* **2007**, *144*, 93–100. [[CrossRef](#)]
41. Ho, Y.-S.; McKay, G. Sorption of dye from aqueous solution by peat. *Chem. Eng. J.* **1998**, *70*, 115–124. [[CrossRef](#)]
42. Anwar, J.; Shafique, U.; Salman, M.; Dar, A.; Anwar, S. Removal of Pb (II) and Cd (II) from water by adsorption on peels of banana. *Bioresour. Technol.* **2010**, *101*, 1752–1755. [[CrossRef](#)]
43. Abdelhafez, A.A.; Li, J. Removal of Pb (II) from aqueous solution by using biochars derived from sugar cane bagasse and orange peel. *J. Taiwan Inst. Chem. Eng.* **2016**, *61*, 367–375. [[CrossRef](#)]
44. Inyang, M.; Gao, B.; Ding, W.; Pullammanappallil, P.; Zimmerman, A.R.; Cao, X. Enhanced lead sorption by biochar derived from anaerobically digested sugarcane bagasse. *Sep. Sci. Technol.* **2011**, *46*, 1950–1956. [[CrossRef](#)]
45. Li, Z.; Xiao, D.; Ge, Y.; Koehler, S. Surface-functionalized porous lignin for fast and efficient lead removal from aqueous solution. *ACS Appl. Mater. Interfaces* **2015**, *7*, 15000–15009. [[CrossRef](#)] [[PubMed](#)]
46. Wang, H.; Gao, B.; Wang, S.; Fang, J.; Xue, Y.; Yang, K. Removal of Pb (II), Cu (II), and Cd (II) from aqueous solutions by biochar derived from KMnO₄ treated hickory wood. *Bioresour. Technol.* **2015**, *197*, 356–362. [[CrossRef](#)] [[PubMed](#)]



© 2020 by the authors. Licensee MDPI, Basel, Switzerland. This article is an open access article distributed under the terms and conditions of the Creative Commons Attribution (CC BY) license (<http://creativecommons.org/licenses/by/4.0/>).